RSC Advances

ROYAL SOCIETY OF CHEMISTRY

www.rsc.org/advances

Physioelectrochemical and DFT investigation of metal oxide/p-type conductive polymer nanoparticles as an efficient catalyst for the electrocatalytic oxidation of methanol

Ali Ehsani[a]*,Mohammad Ghasem Mahjani[b], Ferydon Babaei[c]

Hossein Mostaanzadeh[a],

[a]Departement of Chemistry, Faculty of Science, University of Qom ,Qom, Iran

[b] Department of Chemistry, Faculty of science, K. N. Toosi University of Technology , Tehran, Iran

[c]Department of Physics, Faculty of Science, University of Qom, Qom , Iran

*Corresponding author.

E-mail address: ehsani46847@yahoo.com and a.ehsani@qom.ac.ir (A. Ehsani).

Tel: (009825) 32103038

Fax: (009825) 32854973

Abstract

In the present study, in order to achieve an inexpensive tolerable anode catalyst for direct electrooxidation of methanol, poly tyramine nanoparticles and NiO identified by PTy-NiO, is prepared by in-situ electropolymerization of tyramine in the presence of the anionic surfactant under ultrasonic irradiation. Ni (II) ions are incorporated to electrode by immersion of the polymeric modified electrode having amine group in Ni (II) ion solution and PTy-NiO composite film is formed in the alkaline medium on the surface of the electrode. Surface morphology of the film is studied by surface microscopy techniques. The presence of Nickel in the films is confirmed by energy dispersive spectroscopy (EDS) analysis. Molecular modeling calculations are carried out for polymer-Ni with density functional theory (DFT) level using the 6–31*G* (d,p) basis set and Gaussian 03 program package. Furthermore experimental absorbance spectra of PTy-NiO compared with results obtained from the Maxwell-Garnett theory (MGT) and the value of energy E_g=3.75eV of composite obtained. Modified graphite electrodes (G/ PTy-NiO and G/PTy-SDS-NiO) are examined for their redox process and electrocatalytic activities towards the oxidation of methanol in alkaline solutions. Compared with G/PTy-NiO, G/PTy-SDS-NiO electrode shows a higher catalytic performance in the electrocatalytic oxidation of methanol. A kinetic model was developed and the kinetic parameters were calculated using the methanol concentration dependency of charge transfer resistance derived from the impedance studies.

Keywords: methanol, electrocatalytic, conductive polymer, surfactant, nanoparticles.

1. Introduction

In recent years, electro-oxidation of small organic molecules has attracted much attention due to the development of direct liquid fuel cells, which require highly reactive fuels with high energy density. Methanol is one of the interesting future fuels for fuel cell application. Compared with other cells, the direct methanol fuel cell (DMFC) has several advantages such as high efficiency, very low polluting emissions, a potentially renewable fuel source, fast and convenient refueling, simple operation and ease of fuel storage and distribution. The low operation temperature of a DMFC (typically <95 ◦C) allows for easy start up and rapid response to changes in load or operating conditions [1, 2]. However, compared to the hydrogen based fuel cells, DMFC still remains to be further developed. One of the problems still unsolved is the slow kinetics of methanol oxidation on the fuel cell's anode [3]. Considerable efforts have been directed towards the study of methanol electro-oxidation at high pH. The use of alkaline solutions in a fuel cell has many advantages such as increasing its efficiency [4,5], a wider selection of possible electrode materials, a higher efficiency of both anodic and cathodic processes, almost no sensitivity to the surface structure [6] and negligible poisoning effects in alkaline solutions were observed [7, 8].

In the electrochemical oxidation of methanol, the electrode material is clearly an important factor where a highly efficient electrocatalyst is needed. As described previously [9, 10], a considerable increase in power density and fuel utilization was obtained by optimizing different components of fuel cells. Different electrode materials based on Pt and Pt-binary electrodes were commonly used as a catalyst for the

electrochemical oxidation of methanol. As catalysis is a surface effect, the catalyst needs to have the highest possible surface area. Carbon is a common choice for supporting nanosized electrocatalyst particles in DAFCs because of its large surface area, high electrical conductivity, and pore structures [11, 12]. However, this inert material (carbon) does not help electrocatalytic activities, but serves only as a mechanical support. Therefore, carbon-supported electrodes are generally used as catalyst [11], such as Pt–Ru and Pt–Ru–P/ carbon nano-composites [12], Pt/Ni and Pt/Ru/Ni alloy nanoparticles [13]. It is well established that nickel can be used as a catalyst due to its surface oxidation properties. Many electrodes involving nickel have been used as catalysts in fuel cells. Ni has commonly been used as an electrocatalyst for both anodic and cathodic reactions in organic synthesis and water electrolysis. One of the very important uses of nickel as a catalyst is for the oxidation of alcohols. Several studies of the electro-oxidation of alcohols on Ni have been reported [14-23]. The study of conducting polymer modified electrodes is motivated primarily from the anticipation of a synergistic electrocatalytic benefit from the very good conducting and mechanical properties and their good adhesion to the electrode substrate. Due to their conductivity and stability, both in air and aqueous solution, polypyrrole, polyaniline, polyacetylene, polythiophene, polyindole, poly ortho aminophenol and polythionine has been extensively studied to application in supercapacitor, sensor and catalysis [24-31]. Moreover, the possibility of dispersing metallic particles inside the polymers gives electrodes with higher surface areas, enhanced electrocatalytic activities and facilitates electron transfer due to semi conducting properties [29] and change in Fermi level toward the oxidation of organic molecules [24, 28]. Organic-inorganic composite have attracted considerable attention as

they can combine the advantages of both components and may offer special through reinforcing or modifying each other [28]. Electrodeposition is an effective way to make composite films with a large variety of tunable parameters and so has the advantage of convenient film control.

The purpose of the present work is to preparation of new inexpensive tolerable composite catalyst, characterisation by optical modeling, DFT calculation and study the electrocatalytic oxidation of methanol aiming at the elucidation of the mechanism, derivation of the kinetic parameters of the process and the usefulness of the electrocatalytic process.

2. Computational studies

Computational study has been applied to present optimized structure of the polymer /Ni complex. For phenol derivatives with amino groups, the reported voltammetric studies are interpreted analogy with well-established aniline oxidation, i.e. a E(CE)n mechanism; by which the oxidation of *o*-aminophenol produces a ladder-structured film and reactive intermediates of 2-amino-phenoxazin-3-1 are formed in solution. In the case of tyramine (4-(2-aminoethyl)phenol (Ty), because the amino function is separated from the phenolic ring by two methylene groups, it is expected that only the phenol moiety be oxidized to perform the polymerization [32]. In order to obtain valuable parameters concerning polymerization of tyramine and complex formation with Ni, the polymerization of tyramine was revisited through quantum mechanical DFT calculations. According to EDS results concerning the percentage of Ni in the poly tyramine composite, $[Ni_2\text{heptamer}]^{4+}$ has been selected to optimization. Theoretical calculations were carried

out at density functional theory (DFT) level using the 6–31G (d,p) basis set for all atoms with Gaussian 03 program package for Ni- heptamer. Electronic properties such as highest occupied molecular orbital (HOMO) energy, lowest unoccupied molecular orbital (LUMO) energy and frontier molecular orbital coefficients have been calculated. The molecular sketches of all compounds were drawn using Gauss View 03 [33]. The natural bond orbital (NBO) analysis was applied to determine the atomic charges for Ni-heptamer. Results are presented in Fig. 1 and table 1, 2. The obtained results in Fig. 1 and Table 1 confirmed that the oxidizing phenol moiety performed the polymerization of the tyramine. On the contrary, tyramine has a high electronic density in the phenol moiety related to the $–NH_2$ group. Therefore, dimers can be formed through attacking the cation radical at that position and complex formation with Ni ions was occurred from interaction between $–NH_2$ group and Ni ions Such behavior provides a broad surface with electrostatic anchoring sites, where possible covalent bond formation with ethylamine groups are allowed. Ethylamine groups are very versatile in chemical and conformational senses. A polymer with such characteristics may be used for amplification of the electrochemical response in electrocatalytic processes. The schematic representation of the adsorption behavior of $[Ni_2\text{heptamer}]^{4+}$ on the surface of the electrode is presented in Fig. 1g.

3. Optical modeling

According to our previous works [34-37] optical modeling has been applied to characterization of the composite film. We consider a region $0 \le z \le d$ be occupied by NiO particles dispersed in polymer (PTy) (Fig. 2) while the regions $z \le 0$ and $z \ge d$ are

vacuous. Suppose an arbitrarily polarized plane wave is normally incident (axial excitation) on the chosen structure from $z \le 0$. The phasors of incident, reflected and transmitted electric fields are given as [37, 38]:

$$\begin{cases} \underline{E}_{inc}(\underline{r}) = [a_s \underline{u}_y - a_p \underline{u}_x]\, e^{i K_0 z}, & z \le 0 \\ \underline{E}_{ref}(\underline{r}) = [r_s \underline{u}_y + r_p \underline{u}_x]\, e^{-i K_0 z}, & z \le 0 \\ \underline{E}_{tr}(\underline{r}) = [t_s \underline{u}_y - t_p \underline{u}_x]\, e^{i K_0 (z-d)}, & z \ge d \end{cases} \qquad (1)$$

Where (a_s, a_p), (r_s, r_p) and (t_s, t_p) are the amplitudes of incident plane wave, and reflected and transmitted waves with S- or P- polarizations, $K_0 = \omega\sqrt{\mu_0 \varepsilon_0} = 2\pi / \lambda_0$ is the free space wave number, λ_0 is the free space wavelength, $\varepsilon_0 = 8.854 \times 10^{-12}\, Fm^{-1}$ and $\mu_0 = 4\pi \times 10^{-7}\ Hm^{-1}$ are the permittivity and permeability of free space (vacuum) respectively and $\underline{u}_{x,y,z}$ are the unit vectors in Cartesian coordinates system.

The reflectance and transmittance amplitudes can be calculated, using the continuity of the tangential components of electrical and magnetic fields at interfaces and solving the algebraic matrix equation:

$$\begin{bmatrix} t_s \\ t_p \\ 0 \\ 0 \end{bmatrix} = [\underline{\underline{K}}]^{-1} . [\underline{\underline{M}}] . [\underline{\underline{K}}] . \begin{bmatrix} a_s \\ a_p \\ r_s \\ r_p \end{bmatrix} \qquad (2)$$

The different terms and parameters of this equation are given in detail by Lakhtakia [38]. Herein, the absorbance for natural light is determined as $A = -Log[\frac{T_S + T_P}{2}]$, where $T_i = \sum_{j=s,p} T_{ji}$; $T_{i,j} = \left|\frac{t_i}{a_j}\right|^2$; $i, j = s, p$.

4. Experimental

Tyramine, Sodium hydroxide, lithium perchlorate, nickel nitrate and methanol used in this work were Merck product of analytical grade and were used without further purification. All electrochemical experiments were carried out by an Autolab General Purpose System PGSTAT 30 (Eco-chime, Netherlands). Saturated Calomel Electrode (SCE), a Pt wire and a graphite (G) electrode (0.22 cm^2) were used as the reference, counter and working electrodes, respectively. All studies were carried out at 298 ± 2 K. Microstructure of the electrodeposited composite was studied using different techniques. Scanning electron microscopy (SEM) was performed by a Tescan Vega II HiVac instrument. The transmission electron microscopy (TEM) was performed using a CEM 902A ZEISS transmission electron microscope, with an accelerating voltage of 80 kV.

Films of poly tyramine were formed on the graphite surface using a tyramine monomer solution (0.01 M tyramine in 0.1 M $LiClO_4$ and 0.1M $HClO_4$) and (0.01 M tyramine in 0.1 mol L^{-1} LiClO4, 0.1 mol L^{-1} HClO4 and 0.005 mol L^{-1} sodium dodecyl sulfate (SDS)). The electropolymerization was carried out by potential cycling (40 cycles at a scan rate of 50 mV/s between -0.2 and 0.9 V versus SCE under ultrasonic irradiation. In order to incorporate Ni (II) ions into the PTy film, the freshly electropolymerised graphite electrode was placed at open circuit in a well stirred aqueous solution of 0.1 mol L^{-1} Ni

$(NO_3)_2$. Nickel was accumulated by complex formation between Ni (II) in solution and amines sites in the polymer backbone [30, 31] in a given period of time. The polarization behavior was examined in 1.0 mol L^{-1} NaOH for G/PTy-NiO using cyclic voltammetry. This technique allows the oxide film formation in parallel with inspecting the electrochemical reactivity of the surface. Voltammograms were recorded by cycling the potential between 0.1 and.0.8 V at 100 mV s^{-1} until a stable voltammogram was obtained.

5. Results and discussion

In previous publications [24, 25], we described how poly ortho aminophenol films were electropolymerised in situ on the surface of graphite electrode using cyclic voltammetry methods. Fig. 3a shows the typical multi-sweep cyclic voltammograms during Ty electropolymerization in the absence SDS. As seen in the Fig. 3a, Tyramine (Ty) is oxidized irreversibly at around 650 mV without corresponding cathodic processes in the reverse scan. During the next cycles, one redox peak appears at lower potential, and its current does not considerably increase with potential cycling. This occurred because the soluble products produced on the surface of the electrode did not allow the monomer to reach the electrode and produce more monocation radical. Therefore, a longer potential cycling time is needed for transformation of this to PTy.

By adding 0.005 mol L^{-1} of SDS anionic surfactant to the monomer solution, the monomer oxidation potential was shifted and its oxidation current increased (Fig. 3b). Moreover, the rate of polymerization increased considerably and the redox peaks due to PTy grew (Fig. 3c). Furthermore, under successive potential cycling, their peak currents increased and their growth continued. These results show that, in the presence of SDS,

the monomer can easily reach the electrode surface and produce more monocation radicals. In the case of Ty electropolymerization, the radical cation of Ty monomer is formed on the electrode surface by oxidation of the monomer. This process is considered to be rate determining step. NiOs were formed in the Ni/ polymer backbone after consecutive cycling in the NaOH solution which described in the experimental section.

Fig. 4 shows SEM, TEM images and EDS spectrum of electrosynthesized electroactive film on the surface of the working electrode under ultrasonic irradiation. Nanoparticles of the electroactive polymer in the range of 20-50 nm have been shown in the SEM and TEM micrograph. Formation of the polymer nanoparticles has been related to ultrasonic irradiation effect during electropolymerization of the monomer. The incorporation of Ni in the poly tyramine film is confirmed by the EDS analyses, which shows the presence of Ni located at 7.50, and 8.30 keV (Fig. 4). Also, the EDS spectrum of the electrochemically prepared film shows a signal of carbon (C) at 0.25 keV and oxygen (O) at 0.53 keV characteristic of the PTy polymer. Because the gold is used as a coating in the mounted electrode in SEM analysis we observed also two peak at 2.07 and 9.8 keV of the gold. Thus, the content of Ni ((10.41%) in the film is confirmed by EDS analyses. For showing high active surface area of condutive polymer modified electrode the active surface area of bare graphite and conductive polymer modified graphite electrode were compared by electrochemical probe. Fig. 5 represents cyclic voltammograms bare and modified graphite electrodes in solution of 0.2 M $NaNO_3$ containing 0.002 M $[Fe(CN)_6]^{3-}$ recorded in potential sweep rate 100 mVs^{-1}. Here the electrochemically reversible redox couple ferri/ferrocyanide was used as a suitable probe to examine the active surface area of the films. For analytical purpose, it was assumed that the diffusion of oxidized,

$[Fe(CN)_6]^{3-}$, and reduced species, $[Fe(CN)_6]^{4-}$, in the electrolyte is semi-infinite and one dimensional. The solution initially contains only oxidized species, the bulk concentration of these species being constantly away from the electrode, while the corresponding concentration of reduced species is zero. The supporting electrolyte, $NaNO_3$, is assumed to present at a sufficient concentration so that the contribution of the redox couple to migration can be neglected. Since the PTy synthesized in acidic solution is electroactive when the pH of the medium is less than 4 and is electroinactive when the pH is neutral or basic, under the experimental conditions used, i_{peak} was background corrected so that the only reversible reaction occurring with the redox couple is

$$[Fe(CN)_6]^{3-} + e^- \quad [Fe(CN)_6]^{4-} \qquad (3)$$

The high peak current of this redox in the modified electrode can be related to high surface area of the electroactive polymer.

It is well known that in order to obtain of the effective dielectric constant for dispersed phase volume fractions smaller than $\pi/6$ and the size of features much smaller than the wavelength of the incident electromagnetic wave in the two-component composite medium, we can the Maxwell-Garnett theory (MGT) [40]. In this approximation method, the effective dielectric constant of composite is defined as $\varepsilon_{eff} = \varepsilon_{Pty}(1 - \frac{3f(\varepsilon_{Pty} - \varepsilon_{NiO})}{2\varepsilon_{Pty} + \varepsilon_{NiO} + f(\varepsilon_{Pty} - \varepsilon_{NiO})})$ for NiO particles embedded in PTy, where ε_{Pty} and ε_{NiO} are dielectric constants of PTy and NiO, while f is the volume fraction of dispersed particles. We have used the bulk experimental refractive indexes NiO for homogenization [41]. In our work, we extracted the refractive index k and n of PTy from

absorption coefficient and measured transmittance $k = \alpha\lambda/4\pi$, using Swanepoel model [42, 43] , as shown in Fig. 6. The calculated absorbance spectra as a function of wavelength for NiO particles embedded in PTy are depicted in Fig. 6c. In our calculation for Fig. 6, the structural parameters such as the thickness of composite and the volume fraction of NiO particles, and f_{NiO}=0.1041, respectively, were fixed from the experimental results, respectively. In Fig. 6c, it can be observed that our optical modeling is consistent with experimental results. The plot of $(\alpha h\nu)^2$ vs. photon energy is shown in Fig. 6d. The absorption coefficient was calculated from the absorbance spectra using formula $\alpha = 2.303\frac{A}{d}$, where A is absorbance and $h\nu$ is photon energy. It has been observed that the plot of $(\alpha h\nu)^2$ versus $h\nu$ is linear over a wide range of photon energies indicating the direct type of transitions. The intercept (extrapolation) of this plot (straight line) on the energy axis gives the energy band gap. The value of energy, E_g, of composite was determined E_g = 3.625 eV.

Fig. 7a shows cyclic voltammograms of G/PTy-SDS-NiO electrode in 1 mol L^{-1} NaOH solution in the absence and presence of 0.005 mol L^{-1} methanol at a potential sweep rate of 10 mV s^{-1}. As can be seen in 0.005 mol L^{-1} methanol G/PTy-SDS-NiO electrode generates higher current density for electro-oxidation in NaOH solution. The larger methanol response at the G/PTy-SDS-NiO electrode is due to the composite material which enhances the catalytic properties of nickel oxide through fine dispersion of the catalyst particles into the conductive polymer matrix to results in a drastic increase in surface area. The electrocatalytic behavior of any material depends on various factors such as: (i) the position of the energy levels of the reactive species and the electrode

material; (ii) the charge-transfer process across the electrode/electrolyte interface; (iii) the diffusion of the reactants into/near the electrode surface; and the surface morphology of the electrode. These results may be explained on the basis of electrochemical reactions at a semiconductor electrode. Here, PTy is considered as a p-type semiconductor. The impurity doping level will be situated above the uppermost valence level since PTy is a p-type material. Since the electrode is in an anodic condition, electrons are abstracted from the electrolyte and these combine with holes in the semiconductor. In the present study, it is therefore clear that charge transfer at the electrode/electrolyte interface has the most influence on the electro-oxidation of methanol when using a semi-conducting polymer electrode. It should also be noted that such charge transfer processes are also important in electrochromism and photo-electrochemical effects [44]. In the first step of charge transport within PTy films, which are considered to be p-type semiconductors where holes are majority carriers, there are two processes of importance, inter chain and intra chain transport. The intra chain transport of charge takes place along the main chain, which is facilitated due to extended conjugation. The inter chain charge transport occurs mainly across one chain to the other by hopping mechanism.

Fig. 7b shows cyclic voltammograms of G/PTy-SDS-NiO and G/PTy -NiO electrode in 1 mol L^{-1} NaOH solution in the presence of 0.005 mol L^{-1} methanol at a potential sweep rate of 10 mV s^{-1}. As can be seen in 0.005 mol L^{-1} methanol G/PTy-SDS-NiO electrode generates higher current density and lower potential for electro-oxidation of methanol in NaOH solution. The larger methanol response at the G/PTy-SDS-NiO with respect to G/PTy-NiO electrode is proposed to be the SDS enhances the catalytic properties of nickel oxide through fine dispersion of the catalyst particles into the

conductive polymer matrix to results in a drastic increase in surface area. The histograms of these behavior and difference between different electrodes response are presented in Fig. 7d. According to histogram results, presented composite (G/PTy-SDS-NiO) is more appropriate electrocatalyst for oxidation of methanol than other (bare Ni, G/NiO and G/PT-NiO) in alkaline solution. It is observed that the current density of electro-oxidation of methanol in the surface of G/PTy-SDS-NiO is almost constant in 300 cycles due to the stability of electrocatalyst in this cycle number and indicating that methanol reacted with the surface and no poisoning effect on the surface was observed.

Fig. 7c shows cyclic voltammograms of G/PTy-SDS-NiO electrodes in the 1 mol L^{-1} NaOH solution in the presence of various concentrations of methanol at a potential sweep rate of 10 mV s^{-1}. At G/PTy-SDS-NiO electrodes, oxidation of methanol appeared as a typical electrocatalytic response. The anodic charge increased with respect to that observed for the modified surface in the absence of methanol and it was followed by decreasing the cathodic charge upon increasing the concentration of methanol in solution. In the presence of 0.02 mol L^{-1} methanol with the potential sweep rate of 10 mV s^{-1}, the ratio of anodic to cathodic charge in the presence of methanol was 85/6 while in its absence it was 62/54. Charge is obtained by integrating the anodic and cathodic peaks after background correction.

The anodic current in the positive sweep was proportional to the bulk concentration of methanol (Fig. 7c inset) and any increase in the concentration of methanol caused an almost proportional linear enhancement of the anodic current. So, catalytic electrooxidation of methanol on G/PTy-SDS-NiO seems to be certain. The decreased cathodic current that ensued the oxidation process in the reverse cycle indicates that the

rate determining step certainly involves methanol and that it is incapable of reducing the entire high valent nickel species formed in the oxidation cycle. The electrocatalytic oxidation of methanol occurs not only in the anodic but also continues in the initial stage of the cathodic half cycle. Methanol molecules adsorbed on the surface are oxidized at higher potentials parallel to the oxidation of Ni (II) to Ni (III) species. The later process has the consequence of decreasing the number of sites for methanol adsorption that along with the poisoning effect of the products or intermediates of the reaction tends to decrease the overall rate of methanol oxidation. Thus, the anodic current passes through a maximum as the potential is anodically swept. In the reverse half cycle, the oxidation continues and its corresponding current goes through the maximum due to the regeneration of active sites for adsorption of methanol as a result of the removal of adsorbed intermediates and products. Surely, the rate of methanol oxidation as signified by the anodic current in the cathodic half cycle drops as the unfavorable cathodic potentials are approached.

Chronoamperograms were recorded by setting the working electrode potentials to the desired values and measuring the catalytic rate constant on the G/PTy-SDS-NiO electrode surface. Fig. 8a present chronoamperograms for the G/PTy-SDS-NiO electrode in the absence and presence of methanol over the concentration range of 0.005-0.02 mol L^{-1} . The applied potential step was 650 mV. Plotting the net currents versus the minus square roots of time results in linear dependencies (Fig. 8b inset). Therefore, a diffusion-controlled process is dominant for electrooxidation of methanol. By using the slopes of these lines, we can obtain the diffusion coefficients of the methanol according to the Cottrell equation [45, p. 163]:

$$I=nFAD^{1/2}C^{*}\pi^{-1/2}t^{-1/2} \quad (4)$$

where D is the diffusion coefficient, and C* is the bulk concentration. The mean values of the diffusion coefficients for methanol was 5.16×10^{-6} cm^2s^{-1} on the G/PTy-SDS-NiO surface. Fig. 8c shows compared chronoamperograms of G/PTy-SDS-NiO and G/PTy-NiO electrodes. Chronoamperometry can also be used to evaluate the catalytic rate constant according to [45, p. 503],

$$\frac{I_{cat}}{I_L}=\gamma^{1/2}\left[\pi^{1/2}erf(\gamma^{1/2})+\frac{\exp(-\gamma)}{\gamma^{1/2}}\right] \quad (5)$$

where I_{cat} and I_L are the currents in the presence and absence of the methanol, respectively, and $\gamma = k_0Ct$ is the argument of the error function. k_0 is the catalytic rate constant and t is elapsed time. In cases where $\gamma > 1.5$, erf($\gamma^{1/2}$) is almost equal to unity, and Eq. (5) can be reduced to:

$$\frac{I_{cat}}{I_L}=\gamma^{1/2}\pi^{1/2}=\pi^{1/2}(kC_Mt)^{1/2} \quad (6)$$

From the slopes of the I_{cat}/I_L versus $t^{1/2}$ plots, the mean values of k_0 obtained for methanol was $5.14\times10^{3}cm^3\ mol^{-1}\ s^{-1}$.

Electrochemical impedance spectroscopy is one of the best techniques for analyzing the properties of conducting polymer electrodes and charge transfer mechanism in the electrolyte/electrode interface. It has been broadly discussed in the literature using a variety of theoretical models [46-55]. Fig. 9a shows the Nyquist diagrams of G/PTy-SDS-NiO electrodes recorded at the oxidation peak potential as dc-offset for some

selected concentrations of methanol. Diagrams consist of a small semicircle terminated to depressed capacitive semicircles at low frequency end of the spectrum. The equivalent circuit compatible with the Nyquist diagram [28] recorded in the presence of methanol is depicted in inset of Fig 9b. To obtain a satisfactory impedance simulation of methanol electro-oxidation, it is necessary to replace the capacitor *C* with a constant phase element (*CPE*) in the equivalent circuit. The most widely accepted explanation for the presence of *CPE* behavior and depressed semicircles on solid electrodes is microscopic roughness, causing an inhomogeneous distribution in the solution resistance as well as in the double-layer capacitance. The parallel combination of charge transfer resistance, R_1, and constant phase element, CPE_1, accounts for the injection of electrons from the conductive polymer to the back metallic contact. R_2 and CPE_2 represent the methanol oxidation. To corroborate the equivalent circuit, the experimental data are fitted to equivalent circuit and the circuit elements are obtained. Table 3 illustrates the equivalent circuit parameters for the impedance spectra of methanol oxidation with different concentration of methanol. As can be seen from table3, increasing methanol concentrations decrease the diameters of semicircle, and charge transfer for methanol electrooxidation on the surface of G/PTy-SDS-NiO is lower than G/PTy-NiO. In other words, introduction of SDS into the polymer matrix decrease the charge transfer resistance in Nyquist plots (Fig. 9b).

A number of mechanisms have been proposed for the electro- oxidation of alcohols on Ni in alkaline solutions. While Fleischmann et al. [56] assumed catalytic/intermediate role for NiOOH in the course of an anodic potential sweep.

On the basis of our study and consistent with the literature [28, 57-59] the following mechanism is proposed for the mediated electro-oxidation of methanol on G G/PTy-SDS-

NiO and the corresponding kinetics is formulated. The redox transition of nickel species present in the film is

$$\mathrm{Ni(II)} \xrightarrow{v_1} \mathrm{Ni(III)} + \mathrm{e^-} \quad (7)$$

and methanol is oxidized on the modified surface via the following reaction

$$\mathrm{Ni^{3+}} + \mathrm{methanol} \xrightarrow{v_2} \mathrm{Ni^{2+}} + \mathrm{intermediate} \quad (8)$$

$$\mathrm{Ni^{3+}} + \mathrm{intermediate} \xrightarrow{v_3} \mathrm{Ni^{2+}} + \mathrm{products} \quad (9)$$

where Ni^{3+} sites are regenerated by the power source and on the Ni^{3+} oxide surface by direct electro-oxidation

$$\mathrm{Ni^{3+}\text{-}methanol} \xrightarrow{v_4} \mathrm{Ni^{3+}\text{-}intermediate} + \mathrm{e} \quad (10)$$

$$\mathrm{Ni^{3+}\text{-}intermediate} \xrightarrow{v_5} \mathrm{Ni^{3+}\text{-}products} + \mathrm{e} \quad (11)$$

Eqs. (8) and (9) are according to Fleischmann mechanism and in Eqs. (10) and (11), Ni^{3+} used as active surface for methanol oxidation. Observation of a new oxidation peak for methanol oxidation at a potential much more positive than that of the oxidation of Ni $(OH)_2$ potential is according to Eqs. (10) and (11). According to above equation the Faradic current density can be written as

$$I_F = (v_1 + v_4 + v_5)F \quad (12)$$

In the above sequence of reactions, (7) to (9), k_1 and k_{-1} are obviously potential dependent rate constants and are of the forms:

$$k_1(E) = k_1^{o} \exp\left[\frac{\alpha nF(E - E^{o})}{RT}\right] \quad (13)$$

$$k_{-1}(E) = k_{-1}^{o} \exp\left[\frac{(\alpha - 1)nF(E - E^{o})}{RT}\right] \quad (14)$$

where k^{o}'s are the chemical rate constants measured at equilibrium potential, α being the anodic symmetry factor and other parameters have their usual meanings. The rate laws for the reactions (8) to (10) have the forms of:

$$v_1 = k_1 \Gamma \theta_{II} - K_{-1} \Gamma \theta_{III} \quad (15)$$

$$v_2 = k_2 \Gamma \theta_{III} C^* \quad (16)$$

Where Γ is the total number of adsorption sites per unit area of the electrode surface, θ's represent the fractional coverage's of different nickel valence states and C^* is the bulk concentration of methanol. With only the (II) and (III) valence states of nickel prevailing:

$$\theta_{II} + \theta_{III} = 1 \quad (17)$$

and the rates of changes of their coverage's as well as that of the intermediate compounds being:

$$\frac{d\theta_{II}}{dt} = -\frac{d\theta_{III}}{dt} = -k_1 \theta_{II} + k_{-1} \theta_{III} + k_2 \theta_{III} C^* + k_3 \theta_{III} C_i \quad (18)$$

$$\frac{dC_i}{dt} = k_2 \theta_{III} C^* - k_3 \theta_{III} C_i \quad (19)$$

where C_i is the concentration of intermediate.

Assuming that the steady state approximations dominating:

$$\frac{d\theta_{II}}{dt} = -\frac{d\theta_{III}}{dt} = 0 \quad (20)$$

$$\frac{dC_i}{dt} = 0 \quad (21)$$

one arrives at the values of the coverage's:

$$\theta_{II} = \frac{(k_{-1} + 2k_2 C^*)}{(k_1 + k_{-1} + 2k_2 C^*)} \quad (22)$$

$$\theta_{III} = \frac{k_1}{(k_1 + k_{-1} + 2k_2 C^*)} \tag{23}$$

On the basis of this rate equation the faradic current will be:

$$i_f = \frac{2FAk_1 \Gamma k_2 C^*}{(k_1 + k_{-1} + 2k_2 C^*)} \tag{24}$$

where A being the surface area of the electrode and the corresponding charge transfer resistance is:

$$R_{ct} = \left(\frac{di_f}{dE}\right)^{-1} = \frac{(k_1 + k_{-1} + 2k_2 C^*)^2}{\left[2FA\Gamma k_2 C^* k_1 \left(\frac{2\alpha F k_2 C^*}{RT} + \frac{k_{-1} F}{RT}\right)\right]} \tag{25}$$

the methanol concentrations dependency of R_{ct} are further fitted to Eq. (25) to estimate the values of the rate constants. From this equation the values of the rate constants as k_1=3.86 s^{-1}, k_{-1}=0.31s^{-1} and k_2=1.24×10^3 $cm^3mol^{-1}s^{-1}$ have been calculated.

6. Conclusion

PTy was formed by cyclic voltammetry in monomer solution containing sodium dodesyl sulfate (SDS), on graphite (G) electrode surface. Then, Ni (II) ions were incorporated to electrode by immersion of the polymeric modified electrode having amine group in Ni (II) ion solution. The morphologies and elemental components of the film were inspected by scanning electron microscopy and EDS respectively. Theoretical calculations for Ni-polymerization were carried out at density functional theory (DFT) level using the 6–31*G* (d,p) basis set for all atoms with Gaussian 03 program package. The nickel oxide film was tested for electro-oxidation of methanol in alkaline media. The modified electrodes showed electrocatalytic activity for the oxidation of methanol. A kinetic model was

developed and the kinetic parameters were calculated using the methanol concentration dependency of charge transfer resistance derived from the impedance studies.

Acknowledgements

The authors would like to express their deep gratitude to the Iranian Nano Council for supporting this work.

References

[1] K. Scott, W. M. Taama, P. J. Argyropoulos. J. Power Sources. 1999, **79**, 43-59.

[2] K. Kordesch, G. Simander (1996) Fuel Cells and their Application, VCH Verlagsgesellschaft, Weinheim, p. 151.

[3] TD. Jarvis, EM. Stuve, J. Lipkowski, P. Ross, Electrocatalysis, Wiley-VCH, 1998. p. 109.

[4] R. Parsons,T. Vander Noot. J. Electroanal. Chem. 1988, **257**, 9-45

[5] K. Nishimura, K. Machida, M Enyo. J. Electroanal. Chem. 1988, **251**, 117-125.

[6] E. Morallon, FJ. Cases, JL. Vazquez, A Aldaz. Electrochim. Acta, 1992, **37**, 1883-1886.

[7] PC. Biswas, Y. Nodasaka, M. Enyo. J. Appl. Electrochem. 1996, **26 (1)**, 30-35.

[8] M. Jafarian, RB. Moghaddam, MG. Mahjani, F. Gobal. J. Appl. Electrochem. 2006, **36**, 913-918.

[9] X. Ren, P. Zelenay, S. Thomas, J. Davey, S. Gottesfeld. J. Power Sources. 2000, **86**, 111-116.

[10] T. Schultz, S. Zhou, K. Sundmacher. Chem. Eng. Technol. 2001, **24**,1223-1233.

[11] E. Antolini. Mater. Chem. Phys. 2003, **78 (3)**, 563-573.

[12] WD. King, JD. Corn, OJ. Murphy, DL. Boxall, EA. Kenik, KC. Kwiatkowski, SR. Stock, CM. Lukehart, J. Phys. Chem. 2003, **107(23)**, 5467-5474.

[13] KW. Park, JH. Choi, BK. Kwon, SA. Lee, YE. Sung, HY. Ha, SA. Hong,H. Kim, A. Wieckowski. J. Phys. Chem. 2002, **106 (8),** 1869-1877.

[14] C. Fan, DL. Piron, A. Sleb, P. Paradis. J. Electrochem. Soc. 1994, **141**, 382-387.

[15] IA. Raj, KI. Vasu. J. Appl. Electrochem. 1990, **20(1)**, 32-38.

[16] S . Berchmans, H. Gomathi, GP. Rao. J. Electroanal. Chem. 1995, **394**, 267-270.

[17] M. Fleischmann, K. Korinek, D. Pletcher. J. Electroanal. Chem.1971, **31**, 39-49.

[18] J. Taraszewska, G. Roslonek, J. Electroanal. Chem. 1994, **364**, 209-213.

[19] JR. Allen, A. Florido, SD. Young,S. Daunert, LG. Bachas. Electroanalysis. 1995, **7(8)** 710-713.

[20] A. Bettelheim, BA. White, SA. Raybuck, RW. Murray. Inorg. Chem. 1987, **26(7)** 1009-1017.

[21] X. Tarrus, M. Montiel, E. Valles, E. Gómez, Int. J. Hydrogen. Energ. 2013, **38** ,12774-12785.

[22] M.U. Anu Prathap, R. Srivastava, Nano. Energ. 2013, **2**, 1046-1053.

[23] A. Ehsani, M.G. Mahjani,M. Jafarian, A. Naeemy, Prog. Org. Coat. 2010, **69**, 510-516.

[24] A. Ehsani, M.G. Mahjani, M. Jafarian, Synth. Met. 2011, **161**, 1760-1765.

[25] X-Y. Peng, X-X, Liu, P-J, Hua, D. Diamond, K-T. Lau, J. Solid State. Electrochem. 2010, **14**, 1-7.

[26] M.G. Mahjani, A. Ehsani, M. Jafarian, Synth. Met. 2010, **160**, 1252-1259.

[27] A. Ehsani, M.G. Mahjani, M. Bordbar, R. Moshrefi, Synth. Met. 2013, **165**, 51-55.

[28] A. Ehsani, M. G. Mahjani, M. Jafarian, A. Naeemy, Electrochim. Acta. 2012, **71**, 128-133.

[29] A. Ehsani, M.G. Mahjani, M. Jafarian, Synth. Met. 2012, **62**, 199-204.

[30] R. Ojani, JB. Raoof, S. Fathi, Electrochim. Acta. 2009, **54**, 2190-2196.

[31] F.D. Eramo, J.M. Marioli, A.A. Arevalo, L.E. Sereno, Electroanalysis. 1999, **11**, 481-486.

[32] PC. Biswas, Y. Nodasaka, M. Enyo, J. Appl. Electrochem. 1996, **26**, 30-35.

[33] Gauss View, Version 3.0, Gaussian Inc., Pittsburgh, PA, 2003.

[34] M. Nasrollahzadeh, F. Babei, SM. Sajadi, A. Ehsani, Spectrochim. Acta. A. 2014, **132**, 423-429.

[35] M. Nasrollahzadeh, A. Azarian, A. Ehsani, SM. Sajadi, F. Babaei, Mater. Res. Bull. 2014, **55**, 168–175.

[36] M. Nasrollahzadeh, A. Azarian, A. Ehsani, M. Khalaj, J. Molecular Catalysis A: Chemical, 2014, **394**, 205-210.

[37] A. Ehsani, F. Babaei, M. Nasrollahzadeh, Appl. Surf. Sci, 2013, **283**, 1060-1064.

[38] A. Lakhtakia, R. Messier, Sculptured thin films, Nano engineered Morphology and Optics (SPIE, USA, 2005).

[39] J.H. Choi, Y.H. Lee, C.A. Kim, M.S. J. Mater. Sci. Lett. 2000, **19**, 533-535.

[40]A. Garahan, L. Pilon, J. Yin, Appl J. Phys, 2007, **101**, 014320.

[41] I. Valyukh, S. Green, H. Arwin, G.A. Niklasson, E. Wäckelgard, C.G. Granqvist ,Solar Energy Materials and Solar Cells. 2010, **94**, 724-732.

[42] R. Swanepoe, J. Phys . E: Sci. Instrum. 1983, **16,** 1214-1222.

[43] R. Swanepoel, J. Phys. E: Sci. Instrum,1984, **17**, 896-903.

[44] CSC. Bose, K. Rajeshwar. J. Electroanal. Chem. 1992, **333**, 235-256.

[45] AJ. Bard, LR Faulkner. Electrochemical Methods. Wiley, New York, 2001.

[46] J. Bisquert, J. Electroanal. Chem. 2001, **499**,112-120.

[47] A. Ehsani, M.G. Mahjani, M. Jafarian, Turk. J. Chem. 2011, **35**, 1-9.

[48] A. Ehsani, M.G. Mahjani, M. Bordbar, S. Adeli, J. Electroanal. Chem. 2013,**710**, 29-35.

[49] A. Ehsani, M G. Mahjani, R. Moshrefi, H. Mostaanzadeh, J. Shabani, RSC. Adv. 2014**, 4 (38)**, 20031 – 20037.

[50] A. Ehsani, M. Nasrollahzadeh, MG. Mahjani, R. Moshrefi, H. Mostaanzadeh, Ind. Eng. Chem. 2014, **20**, 4363-4370.

[51] A. Ehsani, M.G. Mahjani, M. Nasseri, M. Jafarian. Anti-Corros. Methods Mater, 2014, **61**, 146-152.

[52] A. Ehsani, F. Babaei, H. Mostaanzadeh, J. Braz. Chem. Soc, 2015, **26**,331-337.

[53] A. Ehsani, M.G. Mahjani, S. Adeli, S. Moradkhani, Prog. Org. Coat. 2014, **77**, 1674-1681.

[54] A. Ehsani, S. Adeli, F. Babaei, H. Mostaanzadeh, M. Nasrollahzadeh, J. Electroanal. Chem. 2014, **713**, 91-97.

[55] A. Ehsani, Prog. Org. Coat, 2015, **78**,133-139.

[56] M. Fleischmann, K. Korinek, D. Pletcher. J.Chem. Soc., Perkin Trans. 2, 1972, **10**, 1396-1402.

[57] M. Jafarian, M.G. Mahjani, H. Heli, F. Gobal, H. Khajehsharifi, M.H. Hamedi, Electrochim. Acta. 2003, **48**, 3423-3429.

[58]A. Ehsani,A. Vaziri-Rad, F. Babaei, H. Mohammad Shiri, Electrochim. Acta. 2015, **159**, 140-148.

[59] A. Ehsani, B. Jaleh, M. Nasrollahzadeh, J. Power Sources. 2014, **257**, 300-307.

Figures and Tables captions

Table 1. Orbital energies for HOMO, LUMO, HOMO-LUMO gap energy (ΔE) and dipole moment (μ) of Compound in the gaseous phase. All quantum chemical parameters calculated at DFT level using the 6-31G(d,p) basis set.

Table 2. Muliken and Natural Charges (e) for atoms.

Table 3. The values of the elements in equivalent circuit represented in Fig. 9 fitted in the Nyquist plots of Fig. 9 and the corresponding relative errors.

Fig. 1. (a) Structure of $[Ni_2heptamer]^{4+}$; (b) Optimized molecular structure of $[Ni_2heptamer]^{4+}$, H atoms have been omitted for clarity; (c) The highest occupied molecular orbital (HOMO) of $[Ni_2heptamer]^{4+}$; (d) The lowest unoccupied molecular orbital (LUMO) of $[Ni_2heptamer]^{4+}$; (e) Muliken charge population analysis and vector of dipole moment of $[Ni_2heptamer]^{4+}$; (f) Natural charge population analysis of $[Ni_2heptamer]^{4+}$ and (g) The schematic representation of the adsorption behavior of $[Ni_2heptamer]^{4+}$ on the surface of the electrode.

Fig. 2. Schematic of the boundary- value problem for optical modeling for NiO/PTy composite film.

Fig. 3. The typical multi-sweep cyclic voltammograms during electropolymerization of PT in the absence SDS (a) and presence SDS (b) and comparison (c).

Fig. 4. SEM, TEM images and EDS of G/PTy-SDS-NiO electrode.

Fig. 5. Cyclic voltammograms for (1) bare graphite and (2) conductive polymer modified electrodes in solution of 0.2 M $NaNO_3$ containing 0.002 M $[Fe(CN)_6]^{3-}$, were recorded in potential sweep rate 100 mVs^{-1}.

Fig. 6. a) Measured transmittance of PTy; b) Extracted refractive index and extinction coefficient for PTy as a function of wavelength; c) Calculated absorbance and $(\alpha h\nu)^2$ for NiO particles dispersed in PTy absorbance vs. wavelength; d) $(\alpha h\nu)^2$ vs. photon energy.

Fig. 7. (a) Cyclic voltammograms in the absence (1) and the presence of 0.005 mol L^{-1} of methanol on G/PTy-SDS-NiO electrode in 1.0 mol L^{-1} NaOH solution. Potential sweep rate was 10 mVs^{-1}. (b) Typical cyclic voltammograms of the (1) G/PTy-NiO and (2) G/PTy-SDS-NiO in1 mol L^{-1} NaOH in the presence of 0.005 mol L^{-1} methanol, Potential sweep rate was 10 mVs^{-1}. (c) Cyclic voltammograms of the G/PTy-SDS-NiO electrode in 1 M NaOH solution in the presence of (1) 0.005 mol L^{-1} ; (2) 0.01 mol L^{-1} ; (3) 0.015 mol L^{-1} ; (4) 0.02 mol L^{-1} ; of methanol in the solution. Potential sweep rate was 10 mVs^{-1}, Inset show dependency of the anodic peak current on the concentration of methanol in solution. (d) Histograms of current density of methanol electrooxidation on the surface of the different Ni-base modified electrodes.

Fig. 8: (a) Double steps chronoamperogram of G/PTy-SDS-NiO electrode in 1 mol L^{-1} NaOH solution with different concentrations of methanol of: (2) 0.005 mol L^{-1} , (3) 0.01 mol L^{-1} , (4) 0.015 mol L^{-1} and (5) 0.02 mol L^{-1} . Potential steps were 600 mV and 360 mV, respectively. (b) chronoamperogram in 0.015 M methanol and dependency of transient current on $t^{1/2}$. Figure 6c shows compared chronoamperograms of G/PTy-SDS-NiO and G/PTy -NiO electrodes in 0.02 mol L^{-1} methanol.

Fig. 9: (a) Nyquist diagrams of G/PTy-SDS-NiO electrode in different concentration of methanol in 1 mol L^{-1} NaOH: (1) 0.005 mol L^{-1} , (2) 0.01 mol L^{-1} , (3) 0.015 mol L^{-1} , (4) and 0.02 mol L^{-1} . DC potential is 600 mV/SCE.(b); Compared Nyquist diagrams of (1) G/PTy-SDS-NiO and (2) G/PTy-NiO electrodes in 0.002 mol L^{-1} methanol in 1.0 mol L^{-1} NaOH, (c) Nyquist plot of G/PTy-NiO in large magnification.

Table 1. Orbital energies for HOMO, LUMO, HOMO-LUMO gap energy (ΔE) and dipole moment (μ) of Compound in the gaseous phase. All quantum chemical parameters calculated at DFT level using the 6-31G(d,p) basis set.

Compound	E_{HOMO}(ev)	E_{LUMO}(ev)	ΔE(ev)	μ(D)
$[Ni_2heptamer]^{4+}$	-10.840	-9.077	1.767	50.6378

Table 2. Muliken and Natural Charges (e) for atoms.

Atom	17N	36N	54N	73N	92N	111N	131N	10O	136Ni	137Ni
Muliken	-0.606	-0.717	-0.732	-0.631	-0.594	-0.604	-0.610	-0.569	0.993	1.030
Natural	-0.921	-0.953	-0.951	-0.923	-0.905	-0.914	-0.925	-0.697	1.180	1.192

Table 3. The values of the elements in equivalent circuit represented in Fig. 7 fitted in the Nyquist plots of Fig. 7 and the corresponding relative errors.

R_s (Ω)	$T_0\times10^5$ ($\Omega^{-1}S^n$)	n_1	R_1 (Ω)	$T_0\times10^4$ ($\Omega^{-1}S^n$)	n_2	R_2 (Ω)	C_m (M)
68.2 (0.36%)	1.22(1.12%)	0.91(0.52%)	45(0.96%)	9.8 (0.98%)	0.76(0.77%)	361(2.35%)	0. 005
67.2 (0.25%)	1.35(0.86%)	0.88(0.23%)	49 (0.75%)	9.4(2.52%)	0.73 (0.13%)	195 (2.15%)	00.01
75.8(0.18%)	1.41(2.14%)	0.89(0.64%)	51 (0.52%)	9.2 (1.65%)	0.78 (0.46%)	128 (1.85%)	0. 0.02

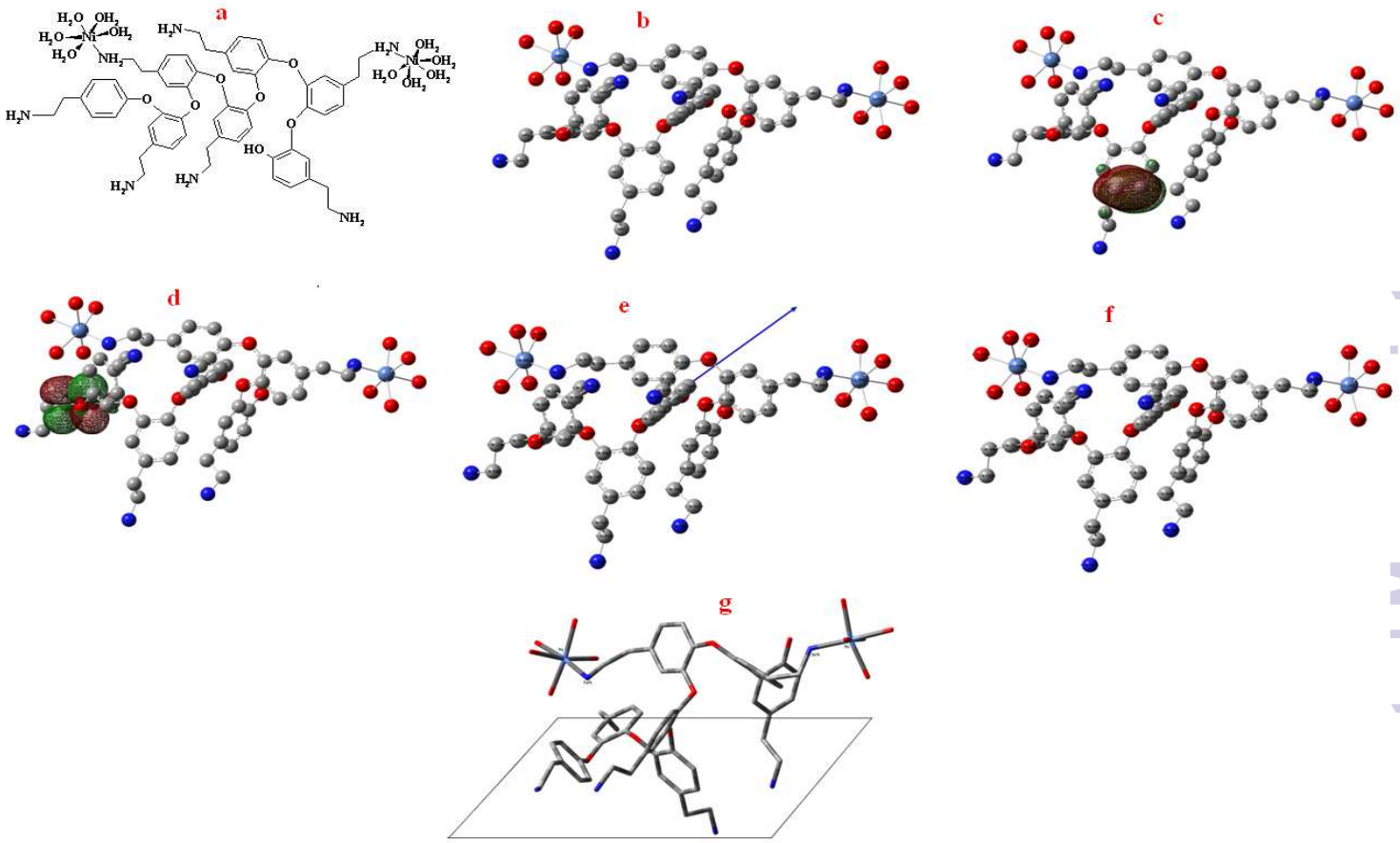

Figure 1

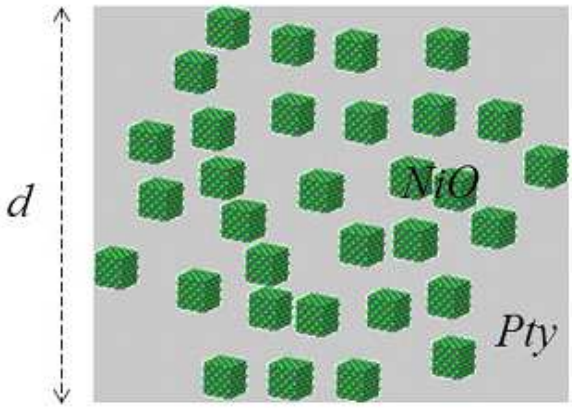

Figure 2

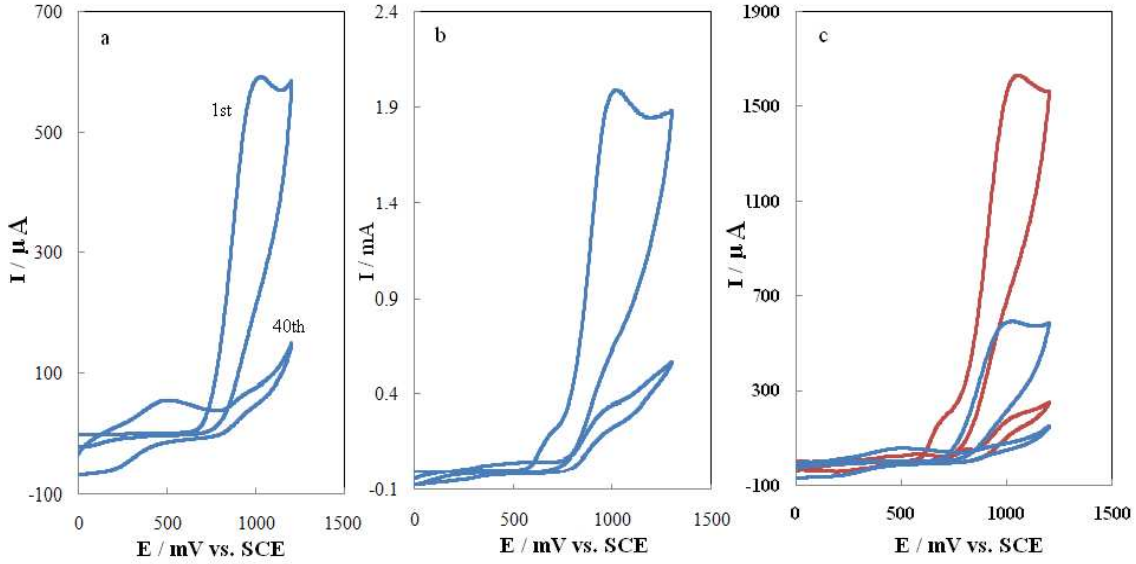

Figure 3

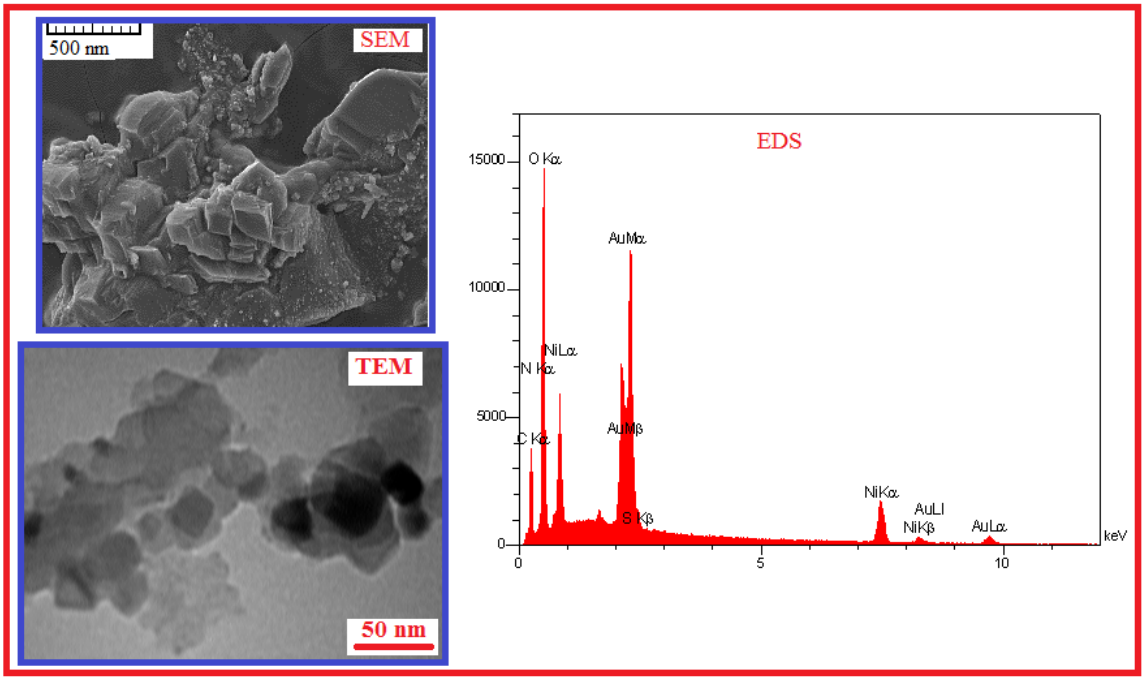

Figure4

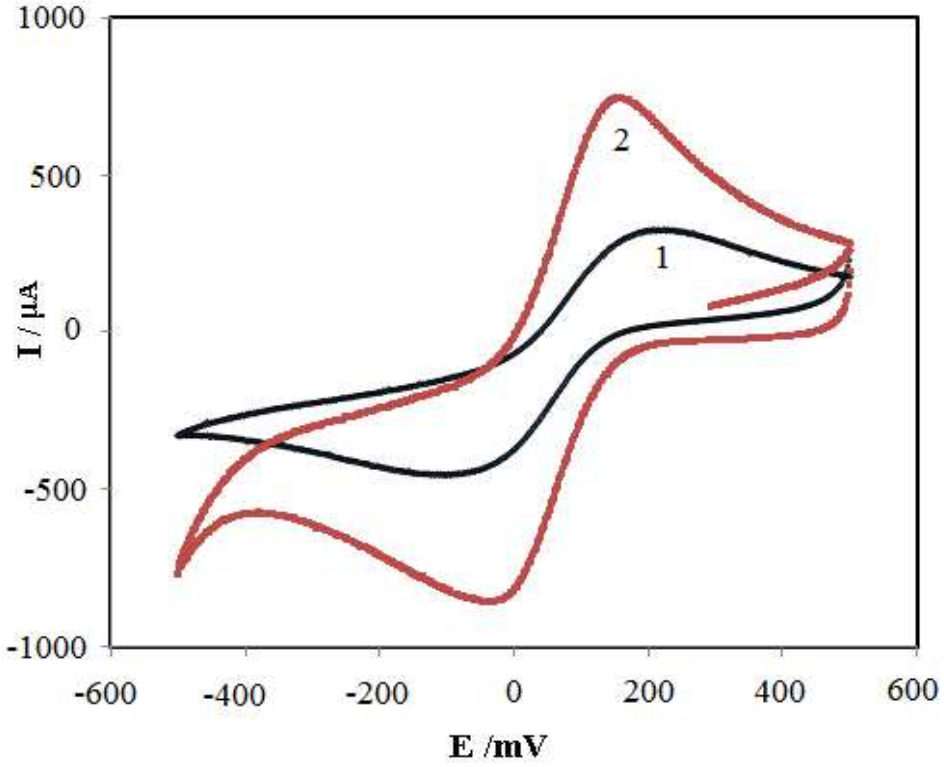

Figure 5

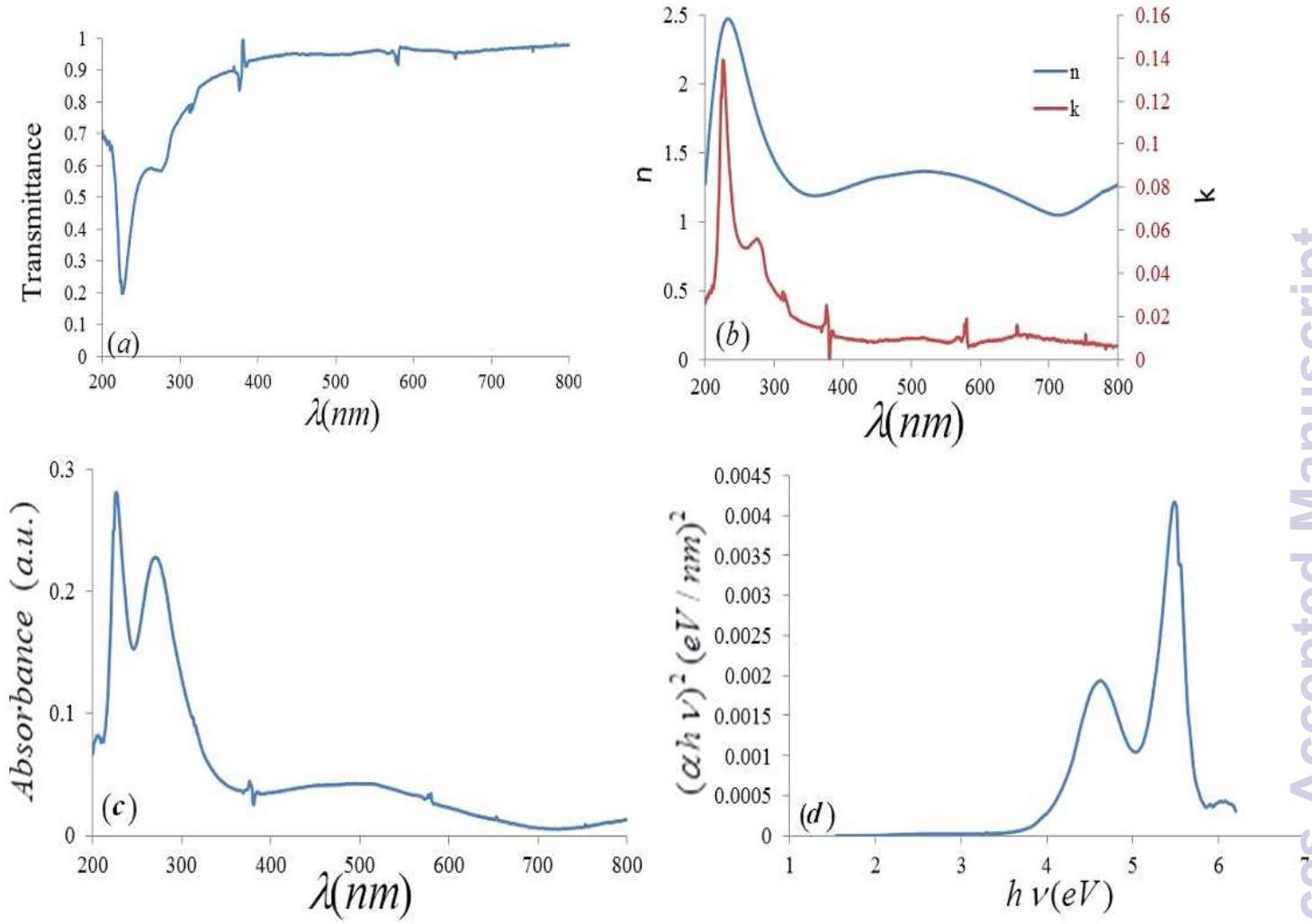

Figure 6

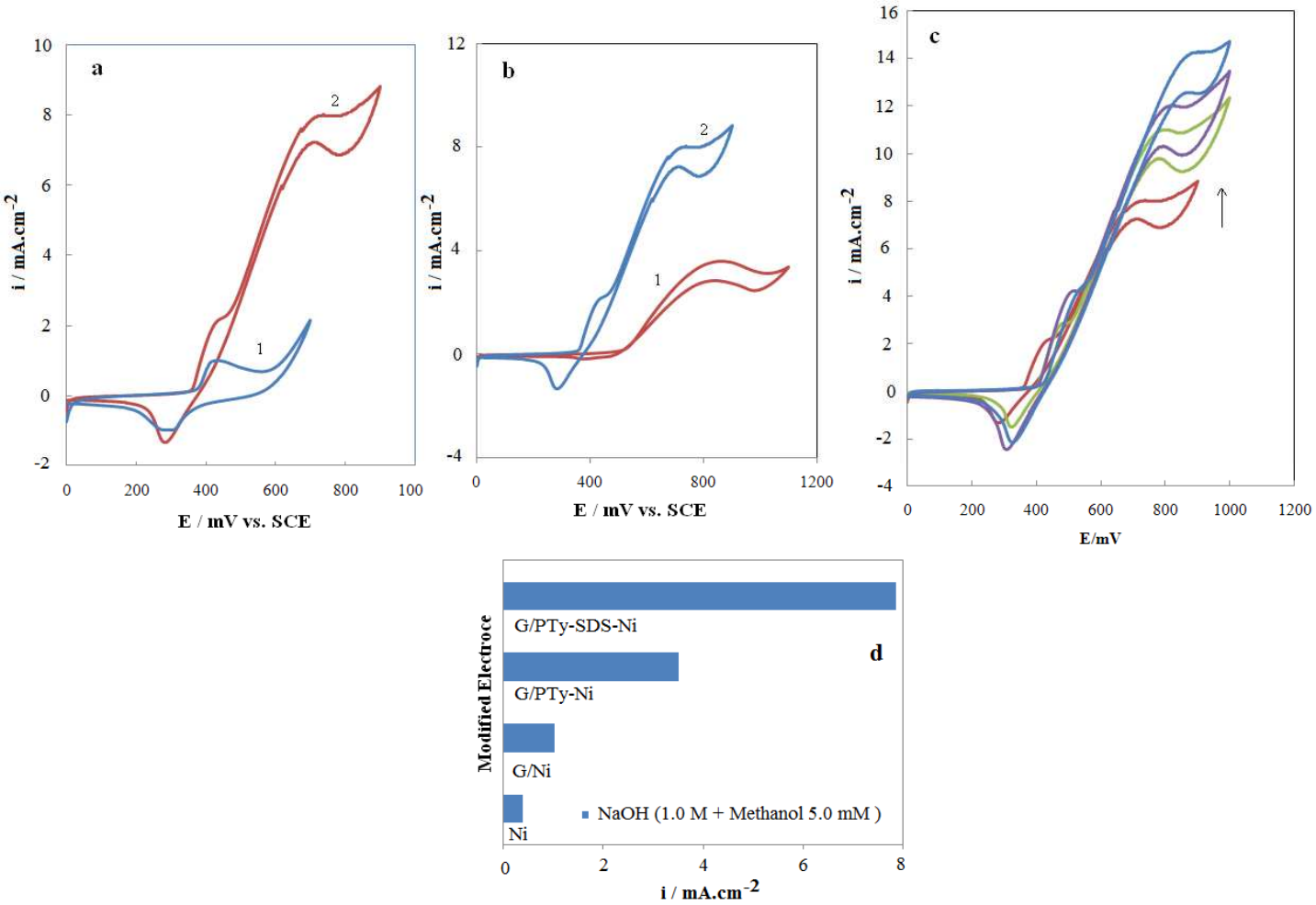

Figure 7

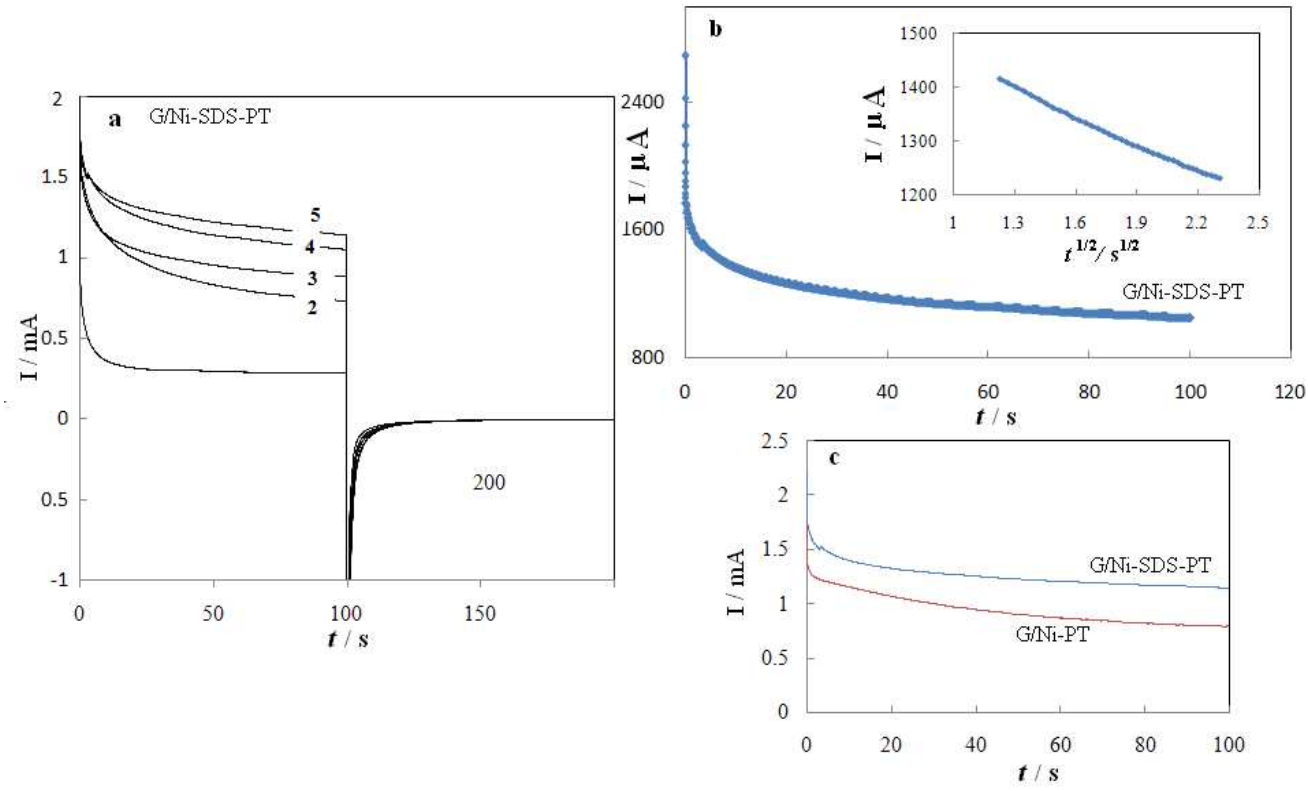

Figure 8

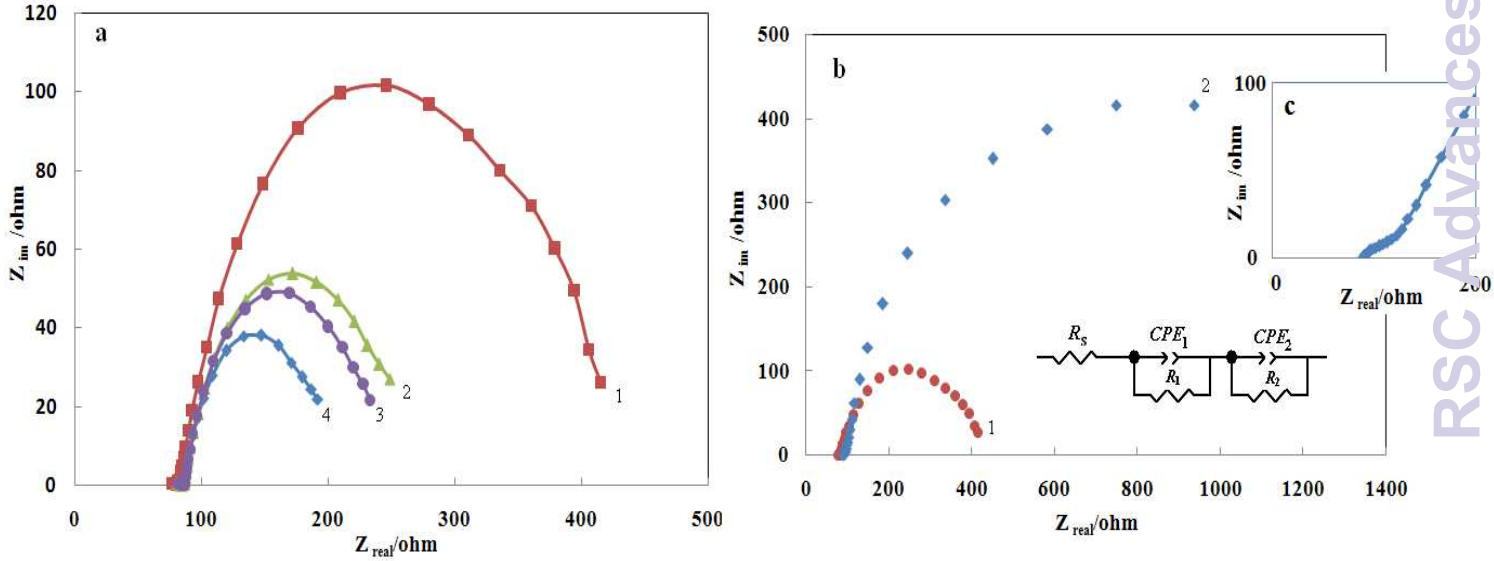

Figure 9

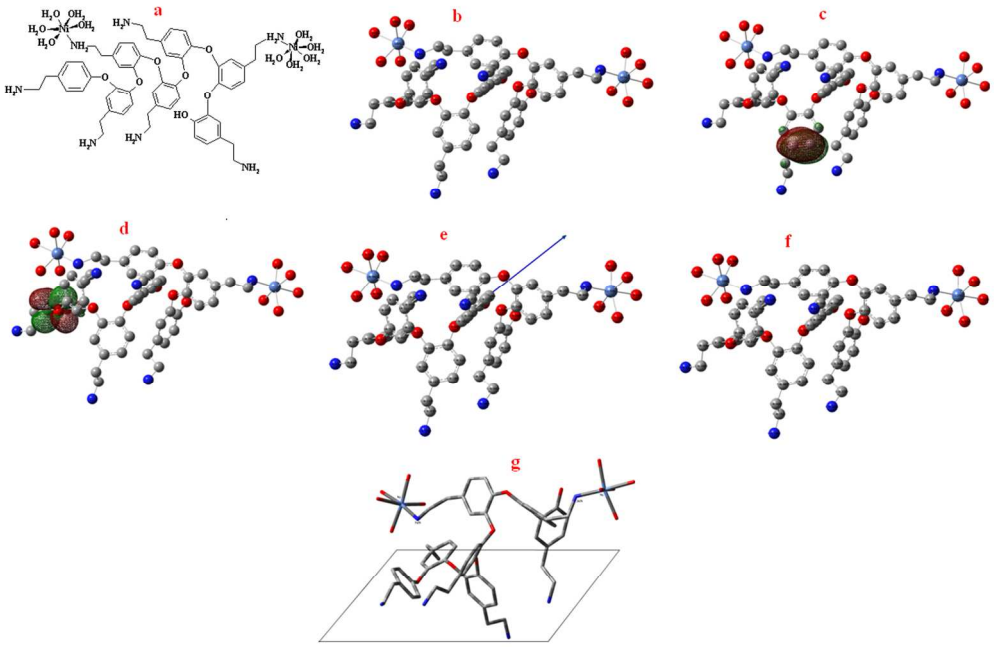

338x228mm (96 x 96 DPI)

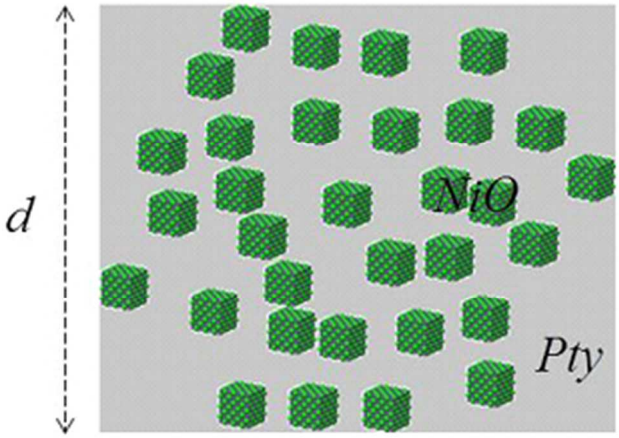

83x61mm (96 x 96 DPI)

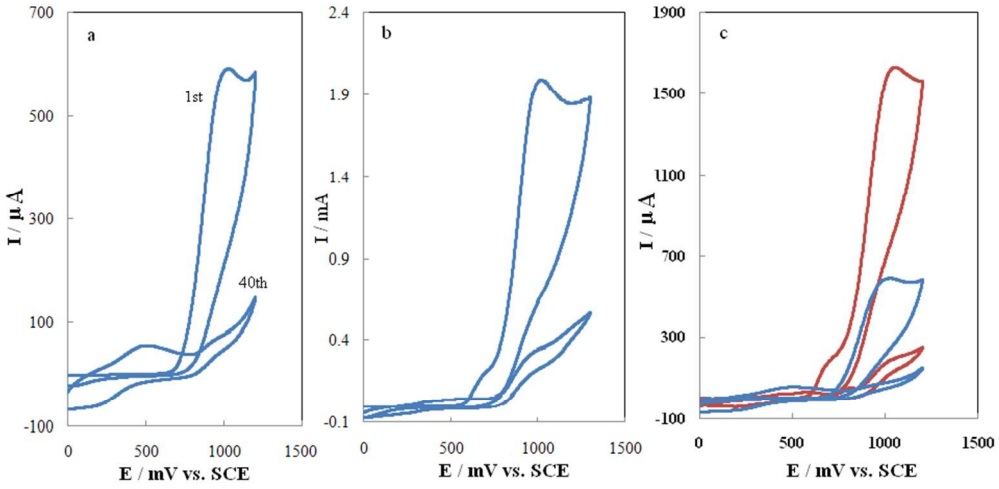

254x131mm (96 x 96 DPI)

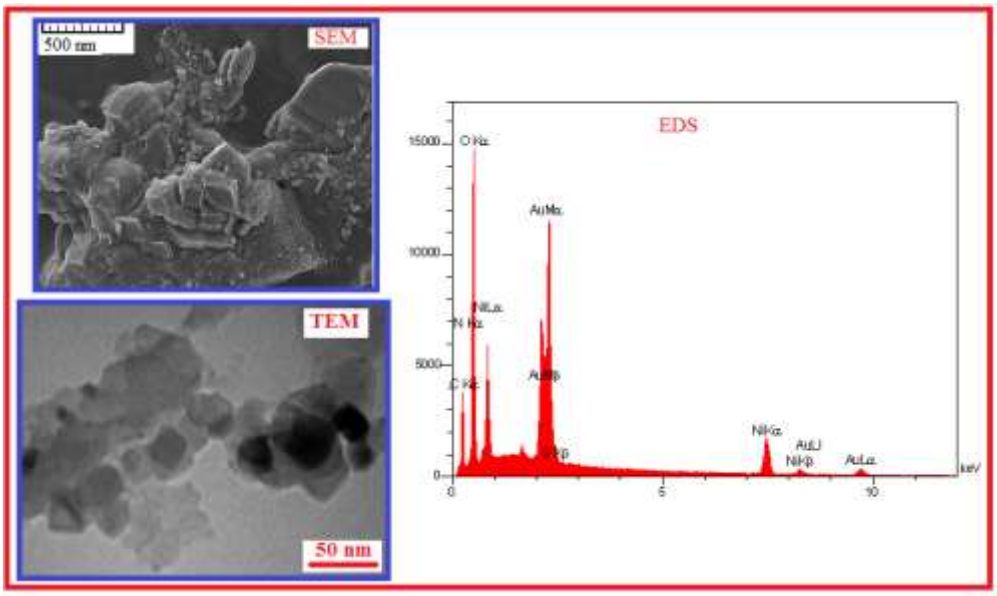

233x138mm (96 x 96 DPI)

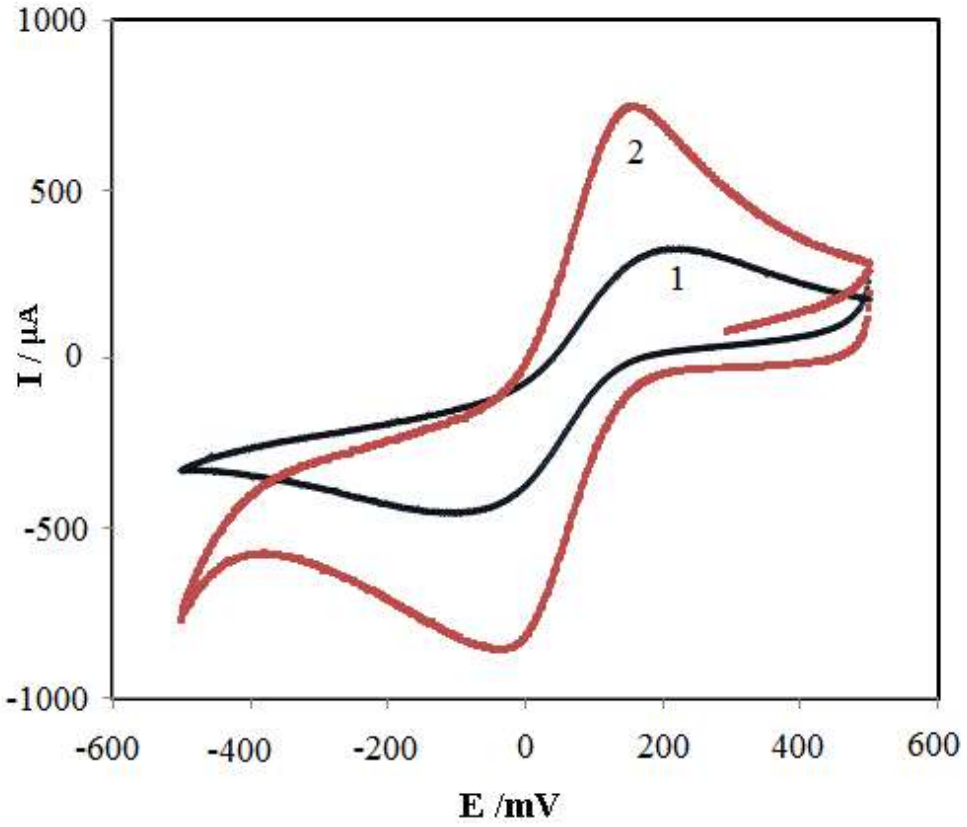

134x113mm (96 x 96 DPI)

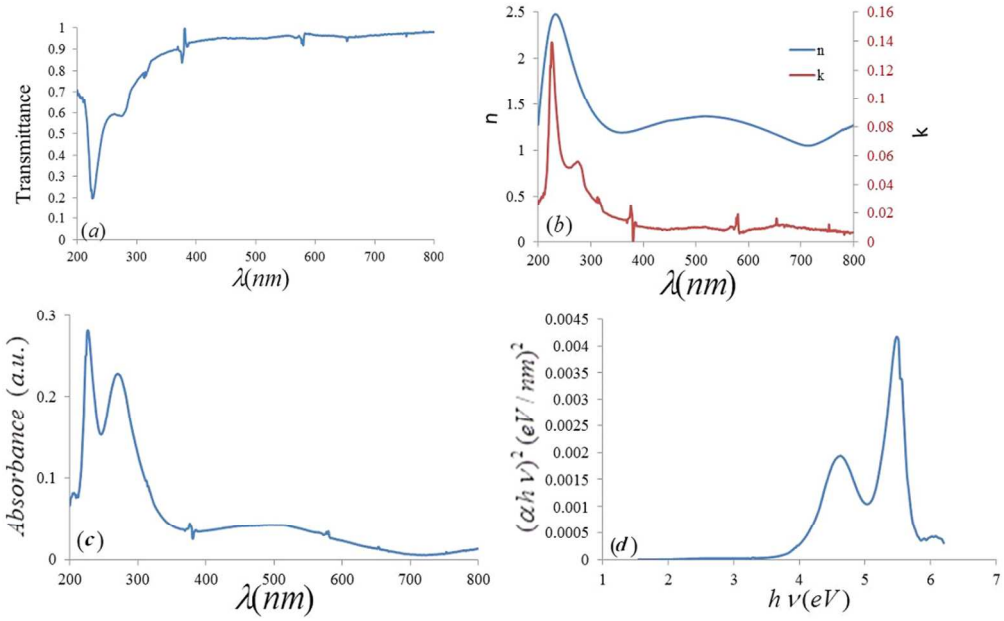

297x189mm (96 x 96 DPI)

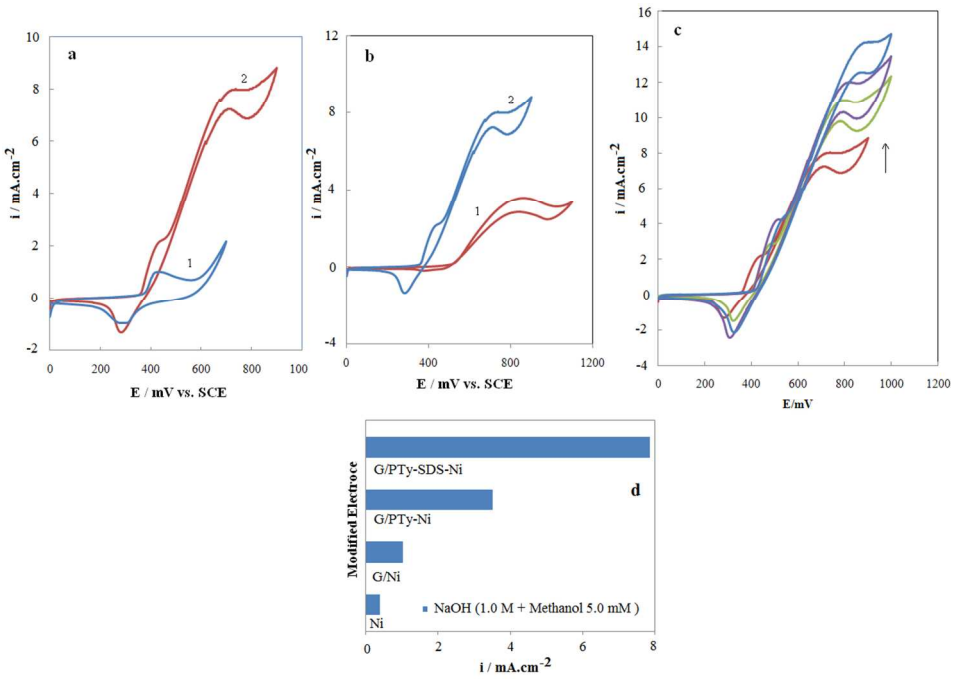

345x238mm (96 x 96 DPI)

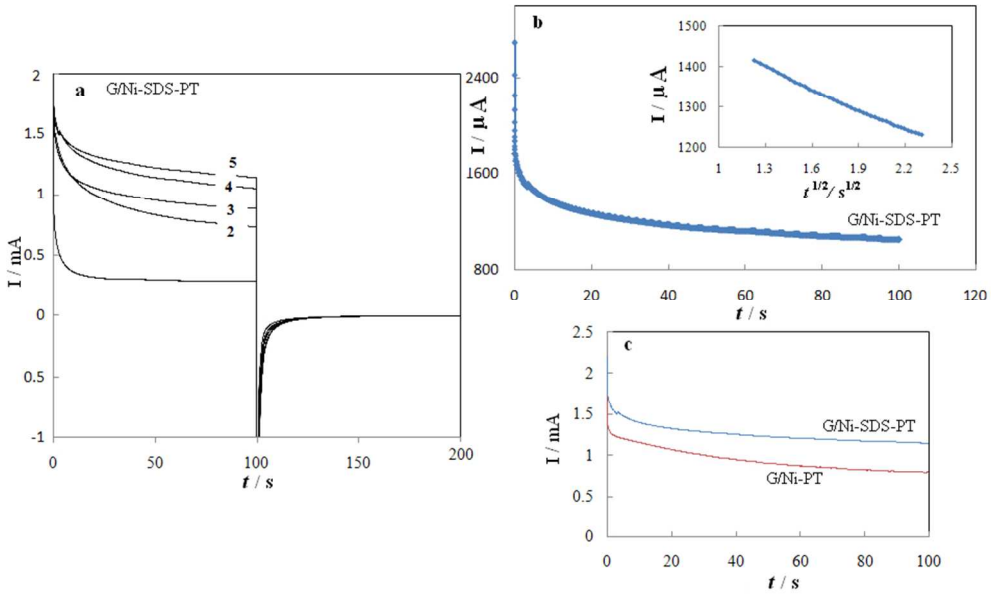

254x156mm (96 x 96 DPI)

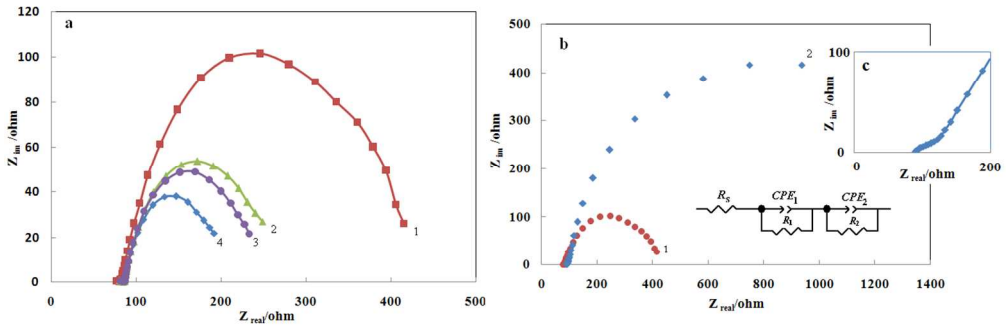

365x124mm (96 x 96 DPI)